IOSR Journal of Mechanical and Civil Engineering (IOSR-JMCE)
e-ISSN: 2278-1684, p-ISSN: 2320-334X, Volume 23, Issue 5 Ser. I (Sep. – Oct. 2026), PP 58-69
www.iosrjournals.org

Correlating Surface Shear Stress to Realistic Complex Terrain in Neutral Atmospheric Boundary Layers

Majed Wardeh[1], Peter J. Disimile[2]
[1]Mechanical and Material Engineering, University of Cincinnati, 2600 Clifton Ave, Cincinnati, OH 45219, United States.
[2]Aerospace Engineering and Engineering Mechanics, University of Cincinnati, 2600 Clifton Ave, Cincinnati, OH 45219, United States.

Abstract
This paper presents computational surface shear stress results of neutral Atmospheric Boundary Layer flow over a domain of complex terrain representative of Cincinnati, Ohio. The computational data, generated using a time averaged turbulence closure model, is used to review flow separation and reattachment patterns, as well as the influence of canopies modelled as surface roughness on the flow behavior. The present data is compared to and combined with a different dataset generated by Large Eddy Simulation to produce an initial correlation that suggests a relation between the geometry of a single hill within a hilly area containing many hills, and the surface shear stress over that single hill. The initial correlation displays a linear pattern between the growth of a hill's downstream slope and the shear stress difference over the slope for small hill slopes. With future improvements to accuracy, the correlation can act as a validation tool for future data measured or computed over complex terrain, and as a relation that explains flow separation and reattachment patterns over complex terrain,
Keywords: *Computational Fluid Dynamics; Turbulence Modelling; Atmospheric Boundary Layer; Complex Topography*

Date of Submission: 09-09-2026 Date of Acceptance: 18-09-2026

I. Introduction

The flow of wind over the surface of complex, non-uniform terrain is defined by separation regions that occur when the flow's boundary layer separates from the surface and forms into a wake. Physical factors, such as gravity and thermal plumes, can drive separation in the Atmospheric Boundary Layer (ABL). A vertical plume driven by a change in heat flux at the surface can perturb the ABL, which is common in unstable ABLs, where the ground is warmer than the air in the ABL and the ABL has a negative vertical temperature gradient. In stable ABLs, where the temperature of the air increases with height, and the ABL has a positive vertical temperature gradient, separation can happen when air flows over non-uniform topography, or man-made buildings and structures, where the surface is not flat and the boundary layer consistently detaches and reattaches to the ground. Near surface separation changes the turbulence characteristics of the flow. As mentioned in a review by Bou-Zeid et al. [6], a change in surface properties stimulates different physical processes at multiple scales in the regions around or downstream of the surface, including turbulence non-equilibrium. Flow separation also influences the air quality by trapping air pollutants in separation regions between hills and valleys [14]. Vertical motions driven by buoyancy are damped in stable ABLs due to thermal stratification, where the positive temperature gradient forces the air into layers that remain stably stratified, which minimizes vertical mixing. Despite the turbulence damping by stratification, shear stress is still substantial at the ground surface, influenced by aspects like vegetation and topography. Arya [3] stated that in nocturnal boundary layers, where negative buoyancy suppresses turbulence, shear becomes the primary local turbulence production mechanism. Mahrt [19] examined turbulence observations collected over 4 months from a short grass site, and found that for a very stable ABL, the dependence of turbulent quantities on the bulk Richardson number becomes weak due to the presence of other processes such as wind fluctuations and gravity waves. Those findings provide that turbulence is never completely suppressed at high Richardson numbers due to shear generation from sub-mesoscale, slowly varying fluctuations, some of which form from friction with the ground and interactions with topography and vegetation. In neutral ABLs, where the air in the ABL maintains a constant temperature throughout the height of the ABL, buoyancy has no contribution to the separation and reattachment of the air flow near the surface due to the absence of heat transfer. In a neutral ABL, separation occurs when the shape of the terrain creates a strong enough pressure gradient that drains the momentum of the overflowing air and forces it to separate from the terrain's surface. The flow's separation point is the point at which the velocity gradient of the air very close to the surface approaches zero. In the case where flow is moving over a hill, the hill's physical features, such as its steepness and curvature, heavily dictate the flow's loss of momentum. The presence of roughness elements on the surface of a hill increases the flow's loss of momentum which also influences flow separation from the surface. Accurately measuring the variation of surface shear over complex terrain can benefit Numerical Weather Prediction (NWP) models in estimating the effects of topographic drag generated by structures such as mountains on large scale circulations in the atmosphere [33].

Multiple prior studies numerically modelled flow over hills in nature at a scale similar to the scale of this study [8, 18, 23, 25, 26], and reported the changes to the ABL velocity profile and turbulent quantities but did not expand on the smaller scale change in surface shear stress. Paiva et. al. [25] and Chavez Arroyo et. al. [8] studied atmospheric flow over natural hills, however, the number of repeated hills in their studies was not numerous enough to produce a conclusion on the behavior of flow over repeated hills. In this paper, shear stress data was generated from Reynolds-Averaged Navier-Stokes (RANS) simulations of a neutral ABL over a computational domain representing a part of Cincinnati, Ohio, where the terrain is complex, made up of repeated hills. From the computational data gathered, a characteristic length for each hill within the terrain and its corresponding surface shear stress were extracted from the simulation and used to produce a correlation. The same characteristic lengths and corresponding shear stresses were extracted from Cooke et. al.'s [10] dataset, which was generated using Large Eddy Simulations (LES) for a neutral ABL over a different complex terrain. The datapoints from both datasets were combined to produce a correlation that presents the trend of seapration and reattachement of flow over repeated complex terrain. Although the results of flow over various canopies will be presented in this paper, the focus of the paper will largely be on the normalization method and the preliminary correlation produced by the combination of the two datasets collected over aerodynamically smooth terrain.

In this paper, hilly terrain will be referred to using the terms "complex" or "heterogeneous." The "roughness" terminology to refer to aerodynamic roughness, also referred to as a canopy, on the surface of the complex terrain, such as grass or sand. The presence of aerodynamic roughness on a surface that is in contact with a flow will influence the flow by changing its boundary layer characteristics. A flow over a smooth surface will develop a viscous sublayer within the boundary layer. The viscous sublayer follows a linear velocity profile, unlike the remainder of the boundary layer which mostly follows a logarithmic velocity profile. The viscous sublayer is where flow perturbations are produced by the instability of the shear mechanism, leading to the generation of turbulence in the flow. However, if the surface is aerodynamically rough, with its roughness elements having a height greater than the height of the viscous sublayer, then the sublayer will cease to exist. When the viscous sublayer ceases to exist, turbulence generation in the boundary layer will no longer be due to the inertial instability of the strain rate, but rather due to pressure drag.

As defined by Schlichting and Gersten [30], the aerodynamic roughness of a surface can be related to the flow using the roughness Reynolds number, Re_k, that is calculated based on the friction velocity of the flow, u_*, and the roughness height, k_s, as $Re_k = \frac{u_* k_s}{\nu}$, with ν being the kinematic viscosity of the fluid. Based on Re_k, three flow regimes have been defined depending on the surface roughness of the wall in a wall-bounded flow:

1) For $Re_k < 5$: The flow is aerodynamically smooth. Turbulence is produced by shear in the viscous sublayer.
2) For $5 \leq Re_k < 70$: The flow is in a transitional phase. The surface holds both smooth and rough wall characteristics.
3) For $Re_k \geq 70$: The flow is fully rough. Turbulence is produced by pressure drag, and skin friction (c_f) is now independent of Reynolds Number.

Flow in the ABL is categorized as continuously aerodynamically rough with Re_k regularly exceeding 70, 32]. The ABL is almost always moving over a rough surface as a rough flow regime, with very few exceptions such as calm winds over a calm ocean surface and weak winds over smooth ice surfaces [2, 31]. In this paper, simulations were completed over a topographically complex terrain for a single smooth surface case, and 5 canopy covered cases with increasing roughness, whos Re_k values of each case are included below in Table 1:

Table 1 Roughness Reynolds number values for each canopy case tested

	Smooth	Sand	Snow	Grass	Wooded Country	Residential
Re_k	≈1	1.06e2	2.70e3	1.95e4	7.24e4	6.12e5

The results of the smooth surface case were the only results thoroughly analyzed for the correlation section of this paper's discussion because the dataset used for comparison to generate the preliminary correlation was generated for a neutral ABL over a smooth surface. Data from the cases with a roughness covered surface are displayed and discussed but not compared to the external dataset. The ABL velocity profile modelled in this paper was measured by Clarke [9] on September 26th 1967 in the northeastern part of the city of Cincinnati, around the Evanston neighborhood. The ABL measured by Clarke [9] was a thermally stable ABL, however, in this study, the ABL was simulated as a neutral ABL, without thermal effects. Thermal effects were removed to simplify the simulations and to allow the data to be comparable to similar neutral ABL over complex topography studies. The span of the boundary layer measurement spanned the early morning starting at 45 minutes before sunrise and ending at 15 minutes after sunrise, during the nocturnal cycle. Although Clarke's ABL data was collected over an area with buildings, all buildings were removed from the present geometry, and only the topography was retained. The boundary layer height was presented as 300 meters with a freestream velocity of 15.2 meters per second. Clarke's ABL's velocity profile was not a logarithmic profile, but was fit it to a logarithmic profile to keep it consistent with Cooke's [10] velocity profile type, which was logarithmic. While a boundary layer height of 300 meters could be considered low for a neutral ABL, neutral ABL heights close to 300 meters have been previously recorded as the lowest end of the neutral ABL height range [32]. The CAD geometry of the area covered by Clarke's experiment was obtained using CADMAPPER.com, which produces a topography scan of a selected geometry, shown in gray in Figure 1 (Images used courtesy of ANSYS, Inc.).

Fig. 1 Simulated Domain Area

II. Numerical Modelling

The topography domain, shown in figure 2, spanned 7000 meters in length (x-direction), and 1000 meters in height (z-direction) from the highest peak. The initial width (y-direction) of the domain was 400 m, however, with the addition of aerodynamic roughness, convergence of the model proved difficult with the current computational resources, so the width of the domain was reduced to reach a minimum continuity convergence of 10^{-5}. A minimum continuity convergence limit of 10^{-5} was deemed sufficient due to the residuals of the quantities of the simulation reaching an asymptote at that limit. The influence of the side boundaries on the data across the domain were examined for three domains, each with a different width, the shear stress across the domain at 4000 meters and 6000 meters downstream from the inlet are shown in figure 3. The tested domains widths were 150, 225, and 275 meters. At 4000 meters downstream from the inlet, the data from every width fluctuated close to the side boundaries, but stayed consistent towards the center of the domain, while at 6000 meters downstream of the inlet, the flow at the center of the domain showed higher fluctuations. Despite the fluctuations, the highest percentage difference between the peak value near the side boundary and the center line value amongst all 6 data lines was 0.84%. The inlet of the domain was set as a velocity inlet, and the outlet was set as a pressure outlet. The side walls and ceiling of the domain were set as symmetry boundaries. All simulations were modelled as isothermal.

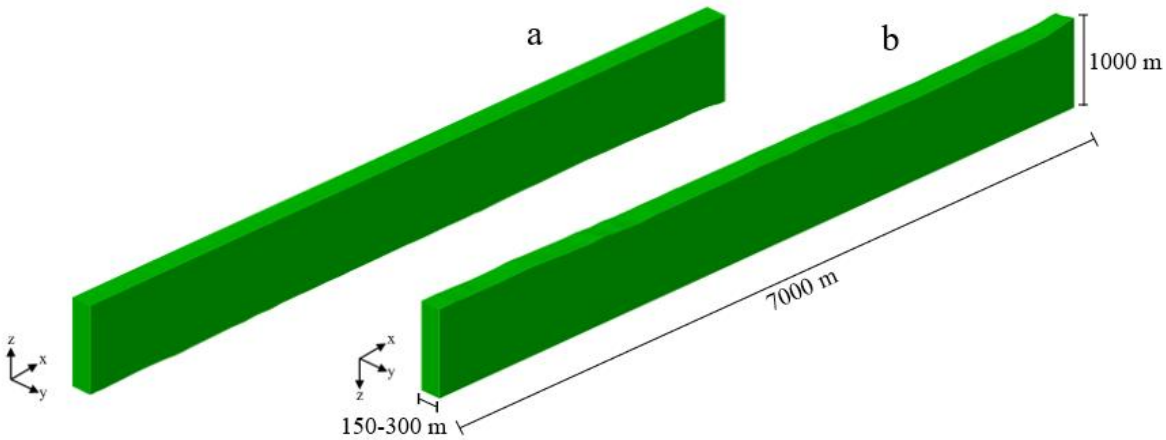

Fig. 2 (a) 3-dimensional domain in the upside direction (b) 3-dimensional domain rotated upside down to show the complex surface

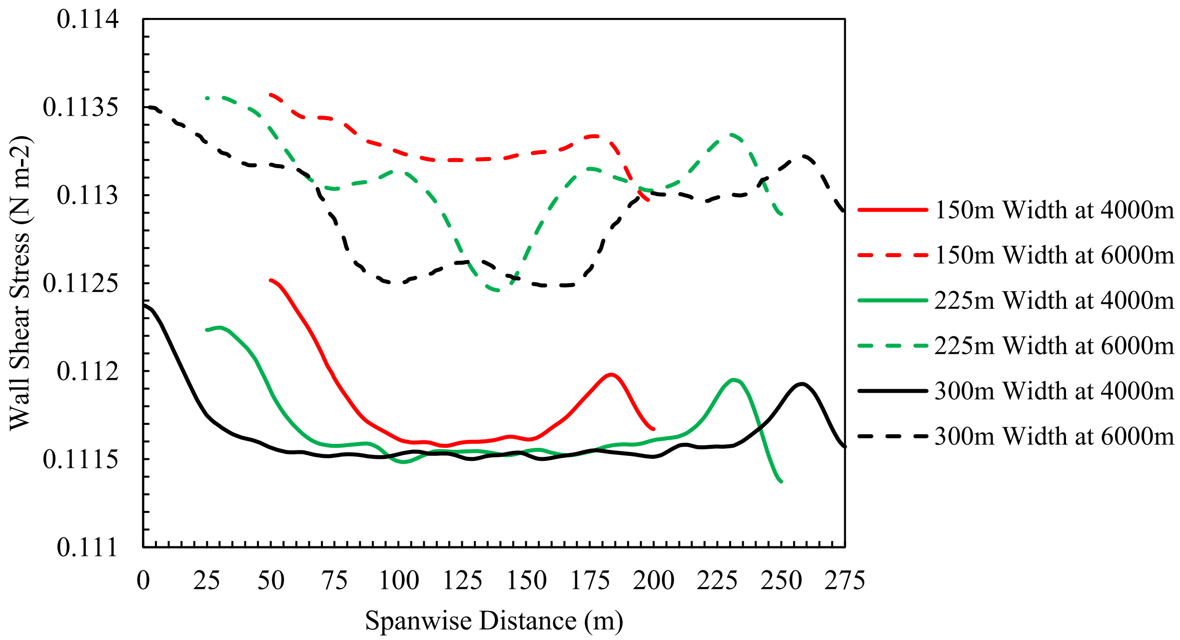

Fig. 3 Shear Stress values plotted across the spanwise direction of the domain at 4000 and 6000 meters downstream from the inlet for different domain widths to test influence of side boundaries. Solid lines represent values collected at 4000 meters downstream of inlet, and dotted lines represent values collected at 6000 meters downstream of inlet.

The model used for the simulations was the Shear Stress Transport (SST) k-ω model developed by Menter [20] which calculates the turbulent kinetic energy (k) and the vorticity (ω) transport equations. The SST k-ω model blends the standard k-ω and k-ε models with a blending function that transitions from calculating k and ω in the near wall region to calculating k and ε in the freestream, ε here being the dissipation rate of k. The SST k-ω model also uses a modified representation of the turbulent eddy viscosity μ_T that includes the strain rate to account for the transport of turbulent shear stress. While it is established that RANS models do not accurately predict near-surface flow behavior in flows over complex terrain, the SST k-ω model is used in this study to explore the viability of an initial correlation that represents flow behavior over complex terrain and not to assert a complete and comprehensive correlation. A previous numerical study by Pieterse and Harms [27] on ABL flow over a single dune showed that the standard k-ε and SST k-ω models produced the closest results to experimental data when evaluated against other RANS models.

The ground of the domain was spatially divided into 2-meter sized mesh elements. The domain contained three vertical mesh regions that were connected by buffer layers, presented in figure 4 (Images used courtesy of

ANSYS, Inc.). Near the ground surface, the mesh is uniformly shaped and very fine in size. The first cell heights above the ground are displayed in Table 2, where the corresponding nondimensional height, z^+, for every case equals 31. A z^+ of 31 means that the mesh skips the viscous sublayer and starts at the beginning of the logarithmic, or inertial region of the boundary layer. Increasing z^+ values were tested for the ABL flow over a flat plate, with the shear results showing little difference in figure 5, confirming that the results were independent of the mesh. The ground mesh then grew vertically for 15 layers at a uniform inflation rate of 1.5, before going through 2 buffer layers that transitioned the mesh to a hexcore form. The cells within the hexcore region grew steadily larger before transitioning into a polyhedral shape that continuously got larger, reaching a size of 128 meters at the ceiling of the domain. The top side of the domain was not the zone of interest of this study, and so it was discretized with a polyhedral mesh as polyhedral meshes have a lower number of cells compared to a cartesian mesh, which reduces the computational power used in the simulations. The mesh was changed according to the aerodynamic roughness applied at the surface for the rough surface cases. The SST k-ω model accounts for surface roughness by modifying the ground boundary condition. The aerodynamic roughness on the surface is input into Ansys Fluent 2023 R2 using the roughness length, k_s. k_s can be found using the aerodynamic roughess height, z_0, using the expression $k_s = \left(\frac{9.793}{C_k}\right) z_0$, where C_k is the roughness distribution constant that accounts for the uniformity of the roughness on the surface. A C_k value of 0.5 was used, indicating that the roughness particles are uniformly distributed over the surface. Since Ansys fluent is a finite volume solver, the software solves every cell at its center point. For the mesh to capture the aerodynamic roughness, the first cell's center point height, z_{center}, should exceed the roughness length, k_s. For that, the first cell height is calculated as the twice z^+ plus twice the roughness height, k_s, which leads the cell's center point to be at $k_s + z^+$. The aerodynamic length (z_0) values for the Snow, grass, and Wooded country were taken from Arya [3], the value for sand was taken from [11] for a mean sand grain size of 0.59 mm, and the value for the residential area was extracted from [17] for a residential area during the fall, around the same season Clarke's ABL profile was measured [9]. The simulations presented in this paper averaged a cell count of 26 million cells.

Surface	z_0 (m)	k_s (m)	First Cell Height (m)	Development Length (m)
Smooth	0	0	0.0024	6000
Sand	0.00025	0.0048965	0.012193	2900
Snow	0.005	0.09793	0.19826	2500
Grass	0.03	0.58758	1.17756	2000
Wooded Country	0.4	1.9586	3.9196	1500
Residential Area	0.66	12.9268	25.856	600

Table 2 Corresponding z_0, k_s, first cell height, and development length for each aerodynamic roughness applied on the domain's surface.

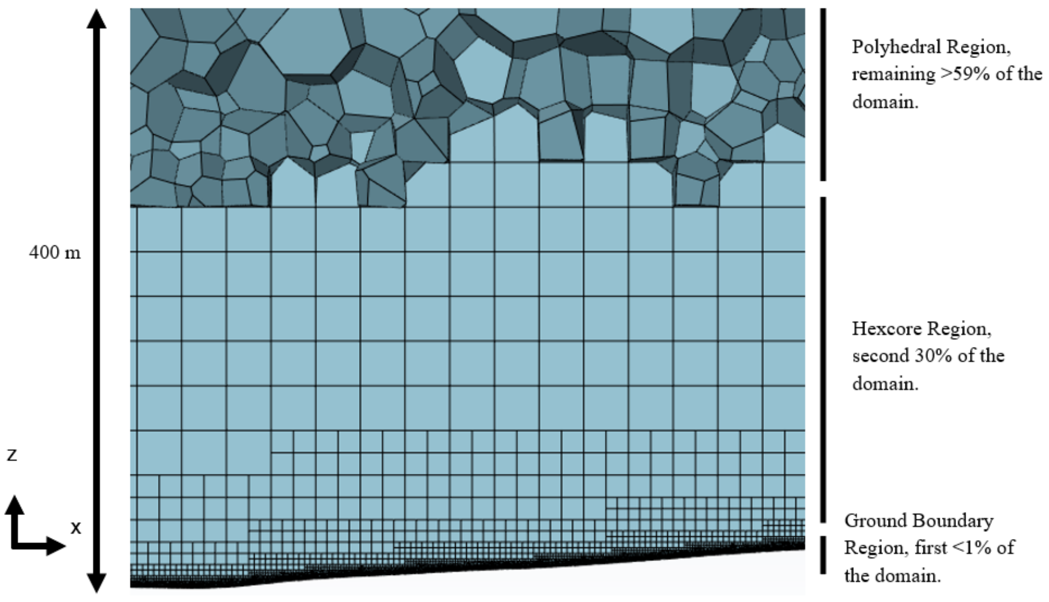

Fig. 4 Cross-Section of the meshed domain. The very fine region near the surface is composed of growing boundary cells. These cells grow into hexcore (square) cells that grow in a ratio of 2:1, before transition into polyhedral cells towards the top of the domain

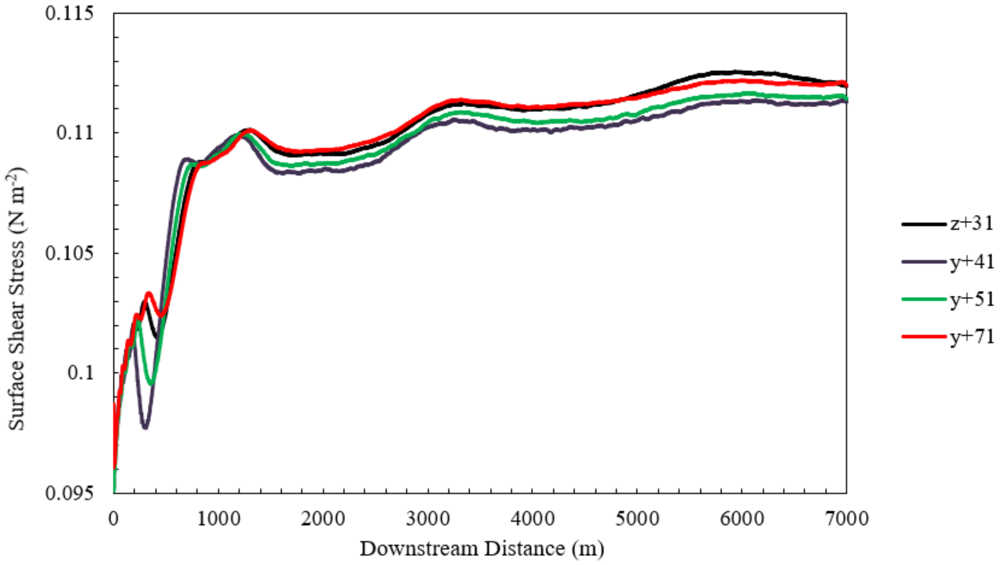

Fig. 5 Examining the sensitivity of the surface shear stress to the change in z^+ by modelling Clarke's ABL over a flat surface. The negligible variation of the data from different z^+ values confirms that the data is independent of the mesh size

Prior to the flow entering the complex topography, a fully developed incoming flow regime was produced. To achieve that, the flow was modelled over a 7000-meter-long flat plate, with identical mesh and boundary conditions to the complex topography domain. At the inlet of both the smooth and aerodynamically rough flat plate domains, a law of the wall-based velocity profile was used that best fit the measured velocity profile extracted from Clarke [9]:

$$u = \frac{u_*}{\kappa} ln(z^+) + 5u_* \tag{1}$$

$$z^+ = \frac{zu_*}{\nu} \tag{2}$$

The inlet velocity profile was fit to match the freestream velocity, $U_\infty = 15.2\ m\ s^{-1}$, at the boundary layer height, $\delta_{ABL} = 300\ m$. The best fitting parameter values were $u_* = 0.351\ m\ s^{-1}$ as measured from the flow over flat terrain simulations, $\kappa = 0.4$ which is von Kármán's constant, and $\nu = 1.7894 \times 10^{-5}\ m^2 s^{-1}$, which is the absolute kinematic viscosity for air at 15° Celsius. The flow becomes fully developed when it behaves in a pseudo-2-dimensional manner. The flow was determined to be fully developed by examining its surface skin friction coefficient as the flow travelled downstream from the inlet and comparing it to existing empirical correlations. The present smooth surface data was compared to experimentally recorded data measured over an aerodynamically smooth surface represented by the Coles-Fernholz [12] correlation, and the present rough surface data was compared to experimentally measured data over an aerodynamically rough surface represented by Pimenta's [28] correlation, both displayed in figure 6.

$$\text{Coles-Fernholz:} \quad c_f = 2\left[\frac{1}{\kappa}\ln\left(\frac{U_\infty \theta}{\nu}\right) + 4.127\right]^{-2} \tag{3}$$

$$\text{Pimenta:} \quad c_f = \frac{2(0.168)}{\left(\ln\left(\frac{864\theta}{k_S}\right)^2\right)} \tag{4}$$

θ in equations 3 and 4 represent the momentum thickness. The Momentum thickness is a theoretical length scale that quantifies the momentum loss within a hydrodynamic boundary layer due to viscous effects that cause the flow within the boundary layer to move slower than the flow in the freestream region, thus resulting in a momentum deficit. The present authors believe that using a laboratory experiment-based skin friction coefficient to validate an ABL's flow's full development increases the margin of uncertainty. Laboratory boundary layers are usually multiple centimeters thick, while ABLs are multiple hundred meters thick. This large resolution of ABLs means that the critical motions within an ABL are measured in large, unlike a laboratory boundary layer where critical motions are measured in detail. However, the available tools that can be used to validate the fully developed flows are the previously mentioned correlations. The percentage differences between the flat plate simulation data and the empirical correlations reach a maximum of 22% in the smooth surface cases. This high percentage difference is again because data from an ABL is being compared to a correlation based off a normal hydrodynamic laboratory boundary layer. An ABL contains greater turbulence than a smaller hydrodynamic boundary layer over a laboratory flat plate. The percentage difference is also due to the high z^+ value, which does not allow the *k-ω* model to calculate the shear within the viscous sublayer. The z^+ value is limited by computational resources, as using a finer z^+ would increase node count and computational requirements. The u_* computed towards the end of the flat plate simulation came out to 0.3 $m\ s^{-1}$, which equated to an Obukhov Length ($L_{Obukhov}$) of 165.7 meters when using Clarke's ABL characteristics [9, 21]. A positive Obukhov length solidifies that the ABL measured by Clarke is a thermally stable one. For $z \ll |L_{Obukhov}|$ wind shear effects are dominant over buoyancy effects [3]. The region of interest for this study, the near surface region, is thus less influenced by buoyancy and more by shear.

III. Normalization Method

The present results were validated with Cooke et al.'s [10] results by finding a pattern between both datasets. By looking at a single hill within the complex terrain, a parameter *H* can be identified, representing the maximum height of the hill, alongside a parameter *L*, which is the remaining width of the hill starting from the horizontal coordinate of the maximum height and ending at the following minimum height. A "slope" or "aspect ratio" *H/L* is created as a unique parameter for every hill in the terrain. This is only applicable for hills with a continuous surface, free of discontinuities, such as smaller topographic bumps within the slope. As for the shear stress analysis, it was determined that using the skin friction coefficient, c_f, which is the surface shear stress normalized by the dynamic pressure, would be unwise. The dynamic pressure only considers the freestream flow velocity and density, both of which scale largely different depending on the characteristics of the ABL examined, such as thermal stability.

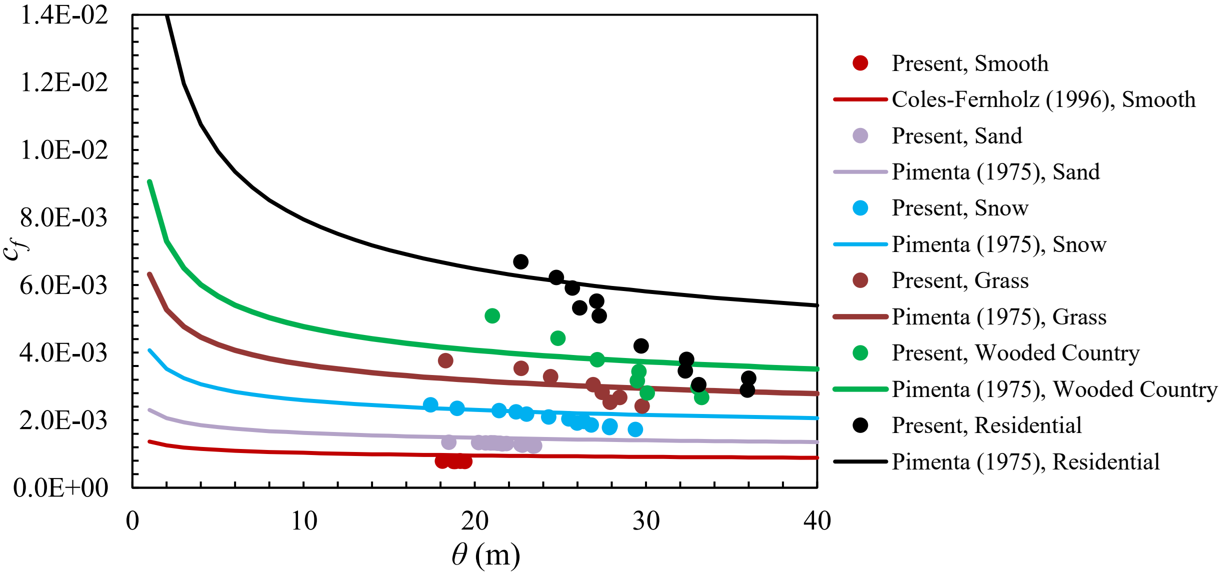

Fig. 6 Comparison of the Flat Plate Simulations Data to the Empirical Correlations of Pimenta and Coles-Fernholz [12,28]

Also, as previously mentioned, using a skin friction correlation that was based off laboratory boundary layers to validate data from an ABL is problematic. Using Cooke et al.'s shear stress normalization, τ/τ_0 , which normalized the shear at any point in the complex domain's surface with the shear measured over the flat plate for the same ABL flow, solves this issue as both shear values are local to the ABL examined. The Aspect ratios of all hills were gathered, alongside the corresponding normalized shear stress at the hilltop and hill bottom, visualized in figure 7, to see if there would be a correlation.

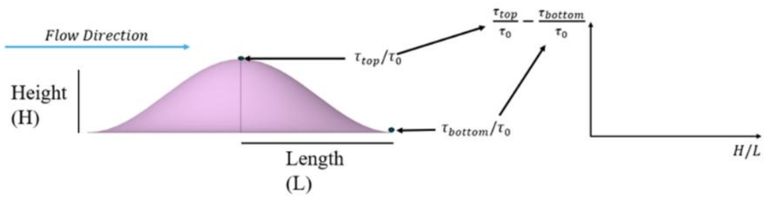

Fig. 7 Visualization of the normalization procedure

The difference between the shear stresses at the hilltop and hill bottom against the aspect ratio of the hill were plotted, with the same being done to Cooke's data. The correlation presented in this paper is produced from shear stress results for ABL flow over a smooth surface generated in this study, combined with shear results for a different smooth surface available in literature. The present rough surface flow data was not used to generate any correlation since there are no similar rough surface studies to compare with, and thus no useful conclusions would be drawn from a rough surface correlation. The rough surface data is provided in figure 8 only to showcase the model's performance when the surface roughness is changed.

IV. Results

The surface shear stress is the main parameter of interest as it is responsible for the turbulence generation within a shear dominated ABL. The surface shear stress data was extracted at the center line between the domain's side walls and was plotted over the length of the domain in figure 8. The hills within the domain are not centered on the center line in between the domain side boundaries. Since the hilly area simulated in this study is a representation of realistic complex terrain, the center line of the domain crosses random locations within the topography, including hillsides. The hilltops are not lined up on the domain centerline, and the center line does not only cross hill maximums or valley minimums. The shear stress values peak at the inlet of the domain due to the incoming flow's instant collision with the complex topography. The shear stress then settles down to a consistent range over the rest of the domain. Data from the first 500 meters of the domain were not used in the present analysis. Examining the how the shear changes with the terrain in figure 8, a greater aerodynamic roughness results in greater shear stress peaks, as suggested in the past by Allen and Brown [1]. However, the peaks around 2100-, 2500-, 4600-, and 6400-meters show that the model predicted a close shear peak value for the wooded country-equivalent roughness and the residential area-equivalent roughness, despite the residential area k_s value being more than 6 times greater than that of the wooded country. This could be owed to the finding that shear stress reaches an asymptote at a certain large k_s, as could be seen in the Moody diagram [22], and in Nikuradse's experiments on flow in pipes roughned by sand grains of uniform size [24]. The shear stress reaching an asymptote physically means that the surface cannot take any more momentum from the flow. By examining the corresponding shear stress to any hilltop in the domain, it is visible that the point at which the maximum shear occurs is not consistent across the different roughness cases. Physically, the shear stress is directly correlated to the near-surface velocity gradient. Wind accelerates as it moves uphill due to the pressure gradient between the flow-facing side and non-flow-facing side of the hill. As the flow sticks to the surface of the hill and accelerates, its friction with the ground increases, increasing the resulting shear stress. The flow continues to stick to the hill until it reaches a point near the hilltop where it encounters a sufficiently large adverse pressure gradient caused by the hill geometry that forces the flow to separate. There is no clear pattern of the flow separating upstream of the hilltop or downstream of the hilltop when changing the surface roughness in figure 8. For example, over the hill at 1600 meters, the maximum shear stress occurs at an earlier point upstream of the hilltop as the surface roughness is increased in each simulated case, signaling that the separation process occurred earlier. On the hill at 1600 meters, the maximum shear stress was recorded at 1625 meters for the smooth case and at 1616 meters for the residential area-equivalent roughness case, a difference of 9 horizontal meters and 0.2 vertical meters. The opposite occurred at the hill at 3500 meters, where the maximum shear stress location varied between the different roughness cases. The highly 3-dimensional turbulent flow formed by the flow separating from the previous hill preceding every successive hill will lead to an inconsistent flow separation location. The absence of shear damping mechanisms formed by factors like thermal instability cause high turbulence intensities in the surface layer of the ABL. The high turbulence intensities will cause the separation locations on hills to be highly random and thus hard to converge into a trend.

In the valleys following the hilltops where separation takes place, the computed shear stress drops significantly. The significant drop is due to the flow losing its momentum from its uphill acceleration and then reattaching to the valley surface at a low velocity. Depending on the hill's aspect ratio and the distance between its peak and the next peak, the flow could skip a valley almost entirely, which can be seen in figure 8 at the valley at approximately 1750 meters, where the difference between the shear stress at the hilltop and subsequent valley is significantly large for the smooth surface case. Additionally, the shear stress at the valley of all the tested aerodynamic roughness cases converge to a similar value, despite their peaks at the hilltop being largely different. It is known that flows over canopies are dominated by large coherent eddies that form due to the hydrodynamic instability following the flow losing its momentum over a climbing hill rather than over a flat surface [13,29]. These large coherent eddies could flow horizontally following a hill peak, entirely skipping the ensuing valley. The phenomenon of the near surface high speed flow skipping a valley is not only due to the aspect ratio but is also dependent on the topography in the area prior to the hilltop. The valleys at 1750 and 2400 meters are both preceded by a chain of rising hilltops. The hilltop prior to the valley at 1750 meters is preceded by a continuously rising hill that climbs 28 meters in elevation uninterrupted. Over the course of the flow climbing the hill and accelerating over it, the flow loses significant momentum due to viscous stresses in case of an aerodynamically smooth surface, or due to pressure drag in case of an aerodynamically rough surface.

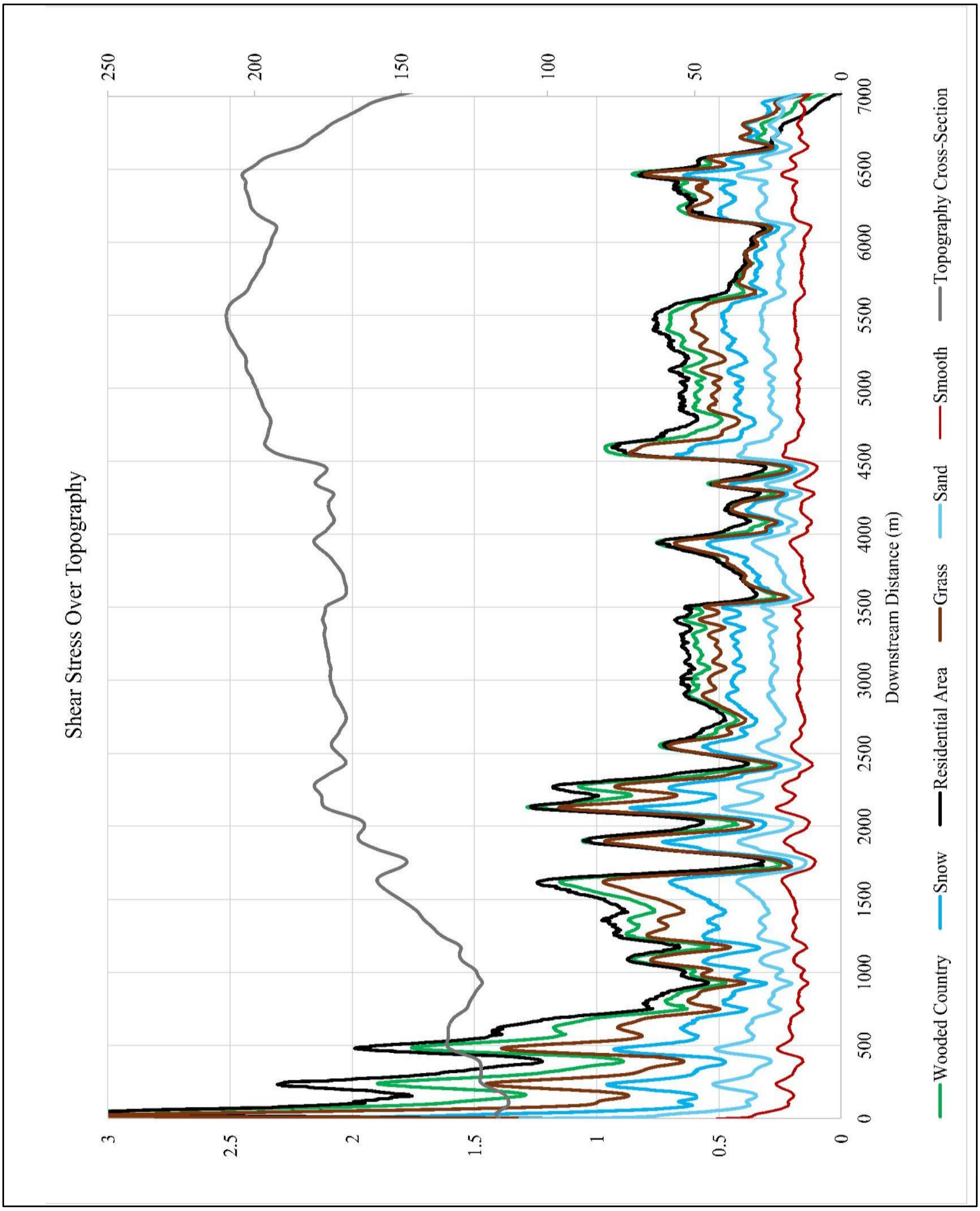

Fig. 8 The surface shear stress plotted over the centerline of the 3D complex topography domain for 6 cases with different aerodynamic roughness at the surface. A cross-section of the topography is plotted in gray. The surface shear stress follows the vertical axis on the left and the topography cross-section follows the axis on the right titled “Ground Elevation”. The ground elevation is relative to sea level

IV.I. Correlation

Following the procedure explained in the normalization section of this paper, figure 9 is produced, combining both present smooth surface RANS data and Cooke et al.'s [10] LES data of a neutral ABL over aerodynamically smooth complex topography. As shown in the figure, both datasets follow a linear pattern with increasing *H/L*, with datapoints from both datasets being concurrently present at an *H/L* < 0.1. Despite both datasets having been collected from simulations over different hilly regions, in different ABLs, and using a different computational method, combining both datasets to produce a linear best fit line turns out with a variance (R2) value of 0.8. A variance value of 0.8 signifies that the best fit line represents 80% of the 27 data points well. The largest data variance occurs around *H/L* = 0.15 where 5 points are more distant from the line. The physical interpretation of this correlation is that, at a low *H/L*, the shear stress difference between the hilltop and hill bottom increases linearly with an increase in *H/L*. However, the higher scatter at higher *H/L* values signifies that the correlation is not universal, and thus, still preliminary. These findings are consistent with Brown et. al. [7], where the authors found that for a neutral flow over sequential cosine hills with a low slope (equivalent to an *H/L* of 0.1 in this paper), the distribution of the shear stress over the downstream side of a hill was linear. The same could not be said for hills at an *H/L* of ~ 0.2, as the distribution began to follow a nonlinear trend in Brown et. al.'s [7] results, with the separation region displaying a recirculation bubble and a further flow reattachment point. Although Brown et. al.'s [7] findings were a result of flow over a sequential series of identical cosine hills, their physical interpretations are found again here when examining the flow over a series of unidentical complex hills. Although RANS models are known to predict separation and reattachment trends inaccurately, figure 9 shows a fair agreement with the LES results, although this cannot be taken as an absolute measure that the RANS model is as good as LES, since this plot is largely macroscopic. Unsteady (fluctuating) results produced using LES are averaged during post-processing and then analyzed statistically, while RANS models directly generate averaged quantities.

The increased spread of data points at a higher *H/L* can be attributed to the increased 3-dimensional turbulence following larger hills, where the flow accelerates up the hill for a longer period, shearing the hill's surface and generating greater turbulence simultaneously. The previous statement is not always true, as *H/L* only represents the hill shape downstream of separation, that is, the side of the hill that is not facing the flow. However, it is very likely that a hill with a high *H/L* has a taller flow-facing side, which forces the flow to shear the surface of the hill longer. Of the present study's hills, 6 out of 9 hills included in the correlation have a taller flow-facing hill side, with 2 out of the 3 not having a taller flow-facing hill side having both sides at a close height. Of the 18 hills examined from Cooke et al.'s study [10], 5 hills had a taller downstream side, 5 hills had a taller upstream side, and 8 hills had both sides at an almost equal height. A more likely reason behind the spread of data is the growth of secondary flows consisting of larger streamwise eddies that are generated as the ABL starts crossing over a complex terrain. The larger streamwise eddies will grow and cause the spanwise mean and fluctuating flow statistics to variate [4,16]. In addition, Ayotte and Hughes suggested [5], from their wind tunnel tests of flow over isolated ridges, that increased turbulent time and length scales produced by a mechanism that scales with the hill width dominate the separation region downwind of a hill.

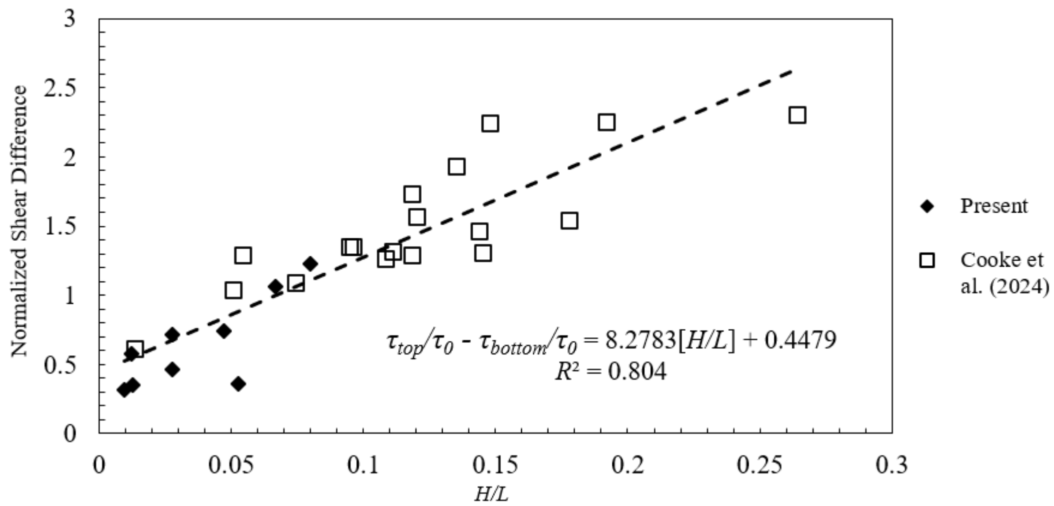

Fig. 9 A combination of the Normalized Shear Difference against *H/L* from both present and Cooke et al.'s [10] data sets

In the present simulations, the streamwise vorticity always had a larger magnitude compared to the spanwise and vertical vorticities in the near-surface region, with the rough surface simulatons having regions of increased spanwise and vertical vorticity in valleys, namely the Residential and Wooded Country roughness cases. The cases with smoother ground surfaces like the snow and sand cases, displayed higher spanwise and vertical vorticity magnitudes, however, the higher magnitudes of vorticity were only within the region extremely close to the wall. In the present smooth surface case, where $Re_k < 1$, the flow displayed smooth flat plate flow charactersitics. The smooth case spanwise vorticity was never high above the first few centimeters from the ground even when flowing over hills, from which it is concluded that the flow separation was very minor. The trend that is present across all cases simulated in this study is that there was increased 3-dimensional vorticity in the valleys following steeper hills, which confirms the suggestion that the increased spread in datapoints at higher *H/L*s can be attributed to higher 3-dimensional turbulence following separation. A drawback of the presented correlation is that a logarithmic ABL velocity inlet profile was utilized to generate both datasets which were used in developing the correlation. It is not guaranteed that using a different velocity inlet profile would would produce similar results for the correlation.

V. Conclusion

This paper presented and analyzed surface shear stress data of ABL flow over complex terrain generated from RANS simulations. The numerical model was introduced and later confirmed to be independent of mesh configuration. The results of the simulations confirmed prior suggestions about the shear generation and momentum loss in the ABL due to complex terrain and canopies. In addition, the results showed no clear pattern of flow separating earlier or later over the hill top depending on surface roughness, which could be a product of high turbulence intensities present in between repeated hills. The need for a comparison tool for the numerical results lead to the creation of a correlation that globalizes shear stress data measured over complex terrain and allows for data points sourced from different ABLs to be compared. The correlation displayed a linear trend of increasing surface shear difference over a single hill situated within repeated complex terrain when the hill's downstream slope is increased. The correlation also allowed for a comparison between the time-averaged turbulence closure model used in this paper, and the LES completed in a prior study. Difficulties remain in the shortage of smooth surface complex terrain shear stress data to further improve the correlation, and in the shortage of shear data over complex terrain covered with roughness elements to develop correlations for various canopy covered heterogeneous terrain.

References

[1]. Allen, T, Brown A (2002) Large-Eddy Simulation Of Turbulent Separated Flow Over Rough Hills. Boundary-Layer Meteorol 102:177–198. https://doi.org/10.1023/A:1013155712154

[2]. Andreas E (1987) A theory for the scalar roughness and the scalar transfer coefficients over snow and sea ice. Boundary-Layer Meteorol 38:159–184. https://doi.org/10.1007/BF00121562

[3]. Arya, SP (1988) Introduction to Micrometeorology. Academic Press, Inc.

[4]. Athanassiadou M, Castro I (2001) Neutral Flow Over A Series Of Rough Hills: A Laboratory Experiment. Boundary-Layer Meteorol 101:1–30. https://doi.org/10.1023/A:1019250801054

[5]. Ayotte KW, Hughes DE (2004) Observations of Boundary-Layer Wind-Tunnel Flow over Isolated Ridges of Varying Steepness and Roughness. Boundary-Layer Meteorol 112:525–556. https://doi.org/10.1023/B:BOUN.0000030663.13477.51

[6]. Bou-Zeid E, Anderson W, Katul GG, Mahrt L (2020) The Persistent Challenge of Surface Heterogeneity in Boundary-Layer Meteorology: A Review. Boundary-Layer Meteorol 177:227–245. https://doi.org/10.1007/s10546-020-00551-8

[7]. Brown AR, Hobson JM, Wood N (2001) Large-Eddy Simulation Of Neutral Turbulent Flow Over Rough Sinusoidal Ridges. Boundary-Layer Meteorol 98:411-441. https://doi.org/10.1023/A:1018703209408

[8]. Chavez Arroyo R, Sanz Rodrigo J, Gankarski K (2014) Modelling of atmospheric boundary-layer flow in complex terrain with different forest parameterizations. Journal of Physics: Conf. Ser. 524. https://doi.org/10.1088/1742-6596/524/1/012119

[9]. Clarke JF (1969) Nocturnal Urban Boundary Layer Over Cincinnati, Ohio. Mon Weather Rev 97(8):582-589. https://doi.org/10.1175/1520-0493(1969)097<0582:NUBLOC>2.3.CO;2

[10]. Cooke J, Jerolmack D, Park GI (2024) Mesoscale structure of the atmospheric boundary layer across a natural roughness transition. Proc of the Natl Academy of Sciences 121(13):e2320216121. https://doi.org/10.1073/pnas.2320216121

[11]. Dong Z, Wang X, Zhao A, Liu L, Liu X (2001) Aerodynamic Roughness of Fixed Sandy Beds. J Geophys Res 106(B6):11001–11011. https://doi.org/10.1029/2001JB900009

[12]. Fernholz HH, Finley PJ (1996) The incompressible zero-pressure-gradient turbulent boundary layer: An assessment of the data. Prog Aerosp Sci 32(4):245-311. https://doi.org/10.1016/0376-0421(95)00007-0

[13]. Finnigan JJ, Shaw RH, Patton EG (2009) Turbulence structure above a vegetation canopy. J Fluid Mech 637:387–424. https://doi.org/10.1017/S0022112009990589

[14]. Finnigan J, Ayotte K, Harman I, Katul G, Oldroyd H, Patton E, . . . Taylor P (2020) Boundary-Layer Flow Over Complex Topography. Boundary-Layer Meteorol 177:247-313. https://doi.org/10.1007/s10546-020-00564-3

[15]. Garratt JR (1994) The Atmospheric Boundary Layer. Cambridge, UK: Cambridge University Press.

[16]. Gong W, Taylor PA, Dornbrack A (1996) Turbulent boundary-layer flow over fixed aerodynamically rough two-dimensional sinusoidal waves. J Fluid Mech 312:1-37. https://doi.org/0.1017/S0022112096001905

[17]. Grimmond C, King T, Roth M, Oke T (1998) Aerodynamic Roughness of Urban Areas Derived from Wind Observations. Boundary-Layer Meteorol 89:1-24. https://doi.org/10.1023/A:1001525622213

[18]. Kim H, Patel V (2000) Test Of Turbulence Models For Wind Flow Over Terrain With Separation And Recirculation. Boundary-Layer Meteorol 94:5-21. https://doi.org/10.1023/A:1002450414410

[19]. Mahrt L (2010) Variability and Maintenance of Turbulence in the Very Stable Boundary Layer. Boundary-Layer Meteorol 135:1-18. https://doi.org/10.1007/s10546-009-9463-6
[20]. Menter FR (1994) Two-Equation Eddy-Viscosity Turbulence Models for Engineering Applications. Am Inst Aeronaut Astronaut Journal 32(8):1598-1905.
[21]. Monin AS, Obukhov AM (1954) Basic laws of turbulent mixing in the surface layer of the atmosphere. Trudy Geofiz Inst AN SSSR 24(151):163–187.
[22]. Moody LF (1944, November) Friction Factors for Pipe Flow. Trans. ASME. 66(8):671–678. https://doi.org/10.1115/1.4018140
[23]. Moreira GA, dos Santos AA, do Nascimento CA, Valle RM (2012) Numerical Study of the Neutral Atmospheric Boundary Layer Over Complex Terrain. Boundary-Layer Meteorol 143:393-407. https://doi.org/10.1007/s10546-011-9694-1
[24]. Nikuradse J (1933) Stromungsgesetze in Rauhem Rohren. (Laws of Turbulent Pipe Flow in Smooth Pipes.). (VDI-Forschungsheft: Germany) 361. (in German)(Translated in NACA Tech. Memo. No. 1292, 1050).
[25]. Paiva LM, Bodstein GC, Menezes WF (2009) Numerical simulation of atmospheric boundary layer flow over isolated and vegetated hills using RAMS. J Wind Eng Ind Aerodyn 97(9-10):439-454. https://doi.org/10.1016/j.jweia.2009.07.006.
[26]. Pattanapol W, Wakes SJ, Hilton MJ, Dickinson KJ (2007) Modeling of surface roughness for flow over a complex vegetated surface. PROC OF WORLD ACADEMY OF SCIENCE, ENG AND TECHNOL 26:273-281.
[27]. Pieterse JE, Harms TM (2013) CFD investigation of the atmospheric boundary layer under different thermal stability conditions. J Wind Eng Ind Aerodyn 121:82-97. https://doi.org/10.1016/j.jweia.2013.07.014
[28]. Pimenta MD (1975) The Turbulent Boundary Layer: An Experimental Study Of The Transport Of Momentum And Heat With The Effect Of Roughness. Dissertation, Stanford University
[29]. Raupach MR, Finnigan JJ, Brunei Y (1996) Coherent eddies and turbulence in vegetation canopies: The mixing-layer analogy. Boundary-Layer Meteorol 78:351–382. https://doi.org/10.1007/BF00120941
[30]. Schlichting H, Gersten K (2017) Boundary-Layer Theory (9th ed.). Springer.
[31]. Smith SD (1988) Coefficients for sea surface wind stress, heat flux, and wind profiles as a function of wind speed and temperature. J Geophys Res 93(C12):15467-15472. https://doi.org/10.1029/JC093iC12p15467
[32]. Stull RB (1988) An Introduction to Boundary Layer Meteorology. Springer Dordrecht. https://doi.org/10.1007/978-94-009-3027-8
[33]. Wood N (2000) Wind Flow Over Complex Terrain: A Historical Perspective and the Prospect for Large-Eddy Modelling. Boundary-Layer Meteorol 96:11–32. https://doi.org/10.1023/A:1002017732694